Analysis, Experimental Results, and Range Adaptation of Magnetically Coupled Resonators for Wireless Power Transfer

Alanson P. Sample, *Student Member, IEEE*, David A. Meyer, *Student Member, IEEE*, and Joshua R. Smith, *Member, IEEE*

***Abstract*—Wireless power technology offers the promise of cutting the last cord, allowing users to seamlessly recharge mobile devices as easily as data are transmitted through the air. Initial work on the use of magnetically coupled resonators for this purpose has shown promising results. We present new analysis that yields critical insight into the design of practical systems, including the introduction of key figures of merit that can be used to compare systems with vastly different geometries and operating conditions. A circuit model is presented along with a derivation of key system concepts, such as frequency splitting, the maximum operating distance (critical coupling), and the behavior of the system as it becomes undercoupled. This theoretical model is validated against measured data and shows an excellent average coefficient of determination (R^2) of 0.9875. An adaptive frequency tuning technique is demonstrated, which compensates for efficiency variations encountered when the transmitter-to-receiver distance and/or orientation are varied. The method demonstrated in this paper allows a fixed-load receiver to be moved to nearly any position and/or orientation within the range of the transmitter and still achieve a near-constant efficiency of over 70% for a range of 0–70 cm.**

***Index Terms*—Adaptive tuning, frequency splitting, magnetically coupled resonators, wireless power.**

I. Introduction

ADVANCES in wireless communication and semiconductor technology have enabled a wide variety of portable consumer electronic, medical, and industrial devices. However, users are still required to manually plug in these mobile devices, limiting ultimate mobility and disrupting use when charge is depleted. Furthermore, as portable devices shrink, connectors become a larger fraction of system size. Wireless power offers the possibility of connector-free electronic devices, which could improve both size and reliability. Thus, there is a desire to use wireless power technology to eliminate the remaining wired power connection.

Manuscript received September 15, 2009; revised January 11, 2010; accepted February 24, 2010. Date of publication March 22, 2010; date of current version January 12, 2011. This work was supported by Intel Labs Seattle.

A. P. Sample is with the Electrical Engineering Department, University of Washington, Seattle, WA 98195-2500 USA, and also with Intel Labs Seattle, Seattle, WA 98105 USA (e-mail: alanson@u.washington.edu).

D. A. Meyer is with the Electrical Engineering and Computer Science Department, Massachusetts Institute of Technology (MIT), Cambridge, MA 02139-4307 USA (e-mail: meyerd@MIT.EDU).

J. R. Smith is with Intel Labs Seattle, Seattle, WA 98105 USA (e-mail: joshua.r.smith@intel.com).

Color versions of one or more of the figures in this paper are available online at http://ieeexplore.ieee.org.

Digital Object Identifier 10.1109/TIE.2010.2046002

Presently, several wireless power techniques are being pursued. It is useful to categorize these efforts in terms of their underlying power-transfer mechanism to understand implications for range, adaptation, and efficiency.

Far-field techniques use propagating electromagnetic waves that transfer energy the same way radios transmit signals. This method has been successfully used to power UHF RFID tags, which have no batteries and an operating range of $\sim$10 m [1], [2]. One of the drawbacks to far-field approaches is the inherent tradeoff between directionality and transmission efficiency. There are many examples of RF and microwave systems that use high-gain antennas to transfer power over kilometer distances at efficiencies of over 90% [3], [4]. These systems suffer from the need for sophisticated tracking and alignment equipment to maintain a line-of-sight (point-to-point) connection in unstructured and dynamic environments.

Alternatively, RF broadcast methods, which transmit power in an omnidirectional pattern, allow for power transfer anywhere in the coverage area. In this case, mobility is maintained, but end-to-end efficiency is lost since power density decreases with a $1/r^2$ dependence, resulting in received power levels many orders of magnitude less than what was transmitted [5].

Inductive coupling (or near-field) techniques do not rely on propagating electromagnetic waves. Instead, they operate at distances less than a wavelength of the signal being transmitted. Applications include rechargeable toothbrushes and the recently proliferating "power" surfaces [6]. These techniques can be very efficient but are limited to transmission distances of about a centimeter. Alternatively, near-field RFID pushes the limit on distance by sacrificing efficiency. Near-field tags have a range of tens of centimeters but only receive power in the microwatt range with 1%–2% transmission efficiency [1].

Previously demonstrated magnetically coupled resonators used for wireless power transfer [7]–[13] have shown the potential to deliver power with more efficiency than far-field approaches, and at longer ranges than traditional inductively coupled schemes. However, this prior work is limited to a fixed distance and orientation, with efficiency falling off rapidly when the receiver is moved away from its optimal operating point.

In this paper, we extend prior analysis of coupled magnetic resonance to elucidate several key system concepts, including frequency splitting, critical coupling, and impedance matching. We present a model of magnetically coupled resonators in terms of passive circuit elements and derive system optimization

0278-0046/$26.00 © 2011 IEEE

Authorized licensed use limited to: MIT Libraries. Downloaded on November 26,2023 at 23:43:08 UTC from IEEE Xplore. Restrictions apply.

APPLE 2029
Masimo v. Apple
IPR2023-00734

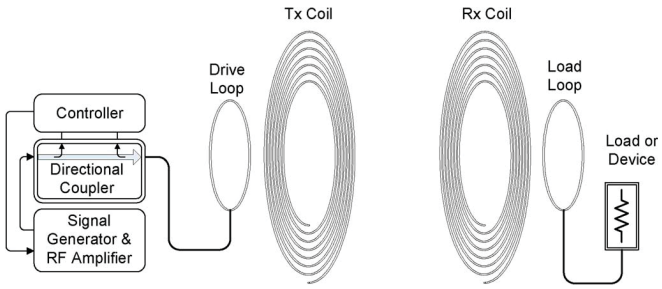

Fig. 1. Sketch of the magnetically coupled resonant wireless power system consisting of an RF amplifier, on the left, capable of measuring the forward and reflected powers. A two-element transmitter, made of a single-turn drive loop and high-Q coil, wirelessly powers the receiver on the right.

parameters. In addition, a method for automatically tuning the wireless power system is demonstrated, so that the maximum possible transfer efficiency is obtained for nearly any distance and/or orientation as long as the receiver is within the working range of the transmitter. This is important from a practical standpoint because, in many applications, such as laptop recharging, the range and orientation of the receive device with respect to the transmit device vary with user behavior [14].

II. System Overview

Fig. 1 shows a diagram of a wireless power system using magnetically coupled resonators. The transmit antenna consists of a single-turn drive loop and a multiturn spiral coil. When the RF amplifier powers the drive loop, the resulting oscillating magnetic field excites the Tx coil which stores energy in the same manner as a discrete LC tank. Another way to think about this two-element transmitter is as a *tuned* step-up transformer, where the source is connected to the primary (the Tx loop) and the secondary (the Tx coil) is left open. The receive side functions in a similar manner, although a load replaces the power source and the system functions as a step-down transformer from the viewpoint of the receive coil.

The key interaction occurs between the two coils, each of which is a high-Q LCR tank resonator. Just as the loop and coil are magnetically coupled, the transmit and receive coils share a mutual inductance which is a function of the geometry of the coils and the distance between them. In order to gain an intuitive understanding of how magnetically coupled resonators can efficiently transfer energy back and forth, it is useful to recall the properties of coupled oscillating systems.

Consider the case of two pendulums connected by a spring, which is analogous to magnetically coupled LCR tanks [15]. In this classic physics example, the two pendulums will form a single system which can oscillate in two modes, one of higher and one of lower frequency than the fundamental frequency of an individual pendulum. Furthermore, the frequency separation of the two modes is dependent on the stiffness (or coupling) of the spring. As this stiffness decreases, the degree of frequency separation (referred to as frequency splitting) also decreases until the two modes converge to the fundamental frequency of a single pendulum. This indicates that, when driving coupled resonators, there can be more than one mode or tuned frequency. This also means that the resonant frequency of the system will change as a function of the coupling, and in the case of the wireless power system, coupling is dependent on the distance between the transmit and receive coils.

Another significant property of coupled oscillators is that the amount of coupling defines the rate of energy transfer, not its efficiency [15]. For the coupled pendulums, the spring constant defines how much energy is transferred from one mass to the other per cycle. The stiffer the spring, the more energy is imparted per cycle; efficiency, on the other hand, is determined entirely by energy losses, due to friction in a pendulum or, equivalently, parasitic resistance in the coils. To the extent that these losses can be neglected, energy not transferred to the receive coil remains in the transmit coil. Thus, even if the coupling is very small (limiting the rate of energy transfer), the efficiency can still be very high, for coils that are high in Q. This is a somewhat counterintuitive result for wireless power systems, particularly when compared to the case of omnidirectional far-field antennas which show a $1/r^2$ dependence for efficiency, and inductive coupling which has a $1/r^3$ dependence.

Finally, the mechanisms for driving and extracting work from coupled resonant systems add additional constraints. To highlight this, the pendulum example can be modified by attaching a dashpot to extract work from one of the masses while sinusoidally driving the other pendulum at one of the system's resonant frequencies. If the amount of power transferred through the spring each cycle is not enough to provide power to the load of the dashpot, the magnitude of the pendulum oscillation will begin to decay. In order to avoid this situation, the stiffness of the spring can be increased so that it imparts more energy per cycle, bringing the system back into equilibrium. This means that, for every load, there is a minimum amount of coupling that is necessary to maintain the system at equilibrium. Equivalently, when driving the wireless power system with an RF source and using a load resistor on the receiver to extract work from the system, the amount of coupling defines how much energy is transferred per cycle. This means that there is a distance (called the critical coupling point) beyond which the system can no longer drive a given load at maximum efficiency.

The following sections will build upon the concepts of frequency splitting, critical coupling, and damping/impedance matching. First, an analytic model of the magnetically coupled resonator system is presented in Section III. This is followed by derivations of key system parameters and figures of merit in Section IV. Section V compares our model and theoretical predictions of system performance to measured results. Finally, Section VI describes adaptive tuning techniques used to achieve near-constant efficiency versus distance while the receiver is within the range of the transmitter.

III. Circuit Model and Transfer Function

The magnetically coupled resonator system can be represented in terms of lumped circuit elements (L, C, and R). Fig. 2 shows a straightforward circuit diagram that can be used for hand analysis or for SPICE simulations.

The schematic consists of four resonant circuits, linked magnetically by coupling coefficients k_{12}, k_{23}, and k_{34}. Starting from the left, the drive loop is excited by a source with finite

Authorized licensed use limited to: MIT Libraries. Downloaded on November 26,2023 at 23:43:08 UTC from IEEE Xplore. Restrictions apply.

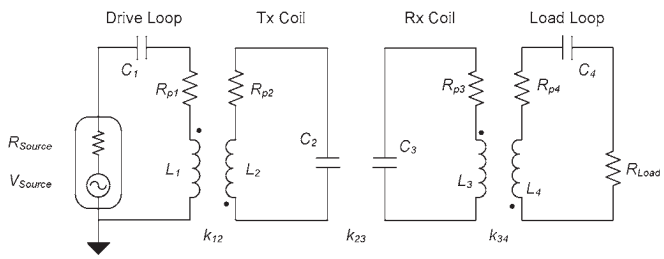

Fig. 2. Equivalent circuit model of the wireless power system. Each of the four antenna elements is modeled as series resonators, which are linked by mutual inductances via coupling coefficients.

output impedance R_{source}. A simple one-turn drive loop can be modeled as an inductor (L_1) with parasitic resistance R_{p1}. A capacitor (C_1) is added to make the drive loop resonant at the frequency of interest. The transmit coil consists of a multiturn air core spiral inductor (L_2), with parasitic resistance (R_{p2}). The geometry of the Tx coil determines its self-capacitance, which is represented as C_2. Inductors L_1 and L_2 are connected with coupling coefficient k_{12}; the receive side is defined similarly. Finally, the transmitter and receiver coils are linked by coupling coefficient k_{23}. A typical implementation of the system would have the drive loop and Tx coil built into a single device such that k_{12} would be fixed. Similarly, k_{34} would also be fixed. Thus, k_{23} is the remaining uncontrolled value, which varies as a function of the distances between the transmitter and receiver.

This circuit model provides a convenient reference for analysis of the transfer characteristics of a magnetically coupled resonator system. For the sake of simplicity, the cross-coupling terms (k_{13}, k_{24}, and k_{14}) are neglected in the following analysis. Section V-A provides a detailed comparison of the accuracy tradeoffs between the simplified model (Fig. 2) and complete model (which includes cross-coupling) versus measured system performance. Next, we return to the simplified model, where Kirchhoff's voltage law (KVL) can be applied to determine the currents in each resonant circuit in (1), where the coupling coefficient is defined in (2)

$$I_1\left(R_{\text{Source}} + R_{p1} + j\omega L_1 + \frac{1}{j\omega C_1}\right) + j\omega I_2 M_{12} = V_s$$
$$I_2\left(R_{p2} + j\omega L_2 + \frac{1}{j\omega C_2}\right) + j\omega(I_1 M_{12} - I_3 M_{23}) = 0$$
$$I_3\left(R_{p3} + j\omega L_3 + \frac{1}{j\omega C_3}\right) + j\omega(I_4 M_{34} - I_2 M_{23}) = 0$$

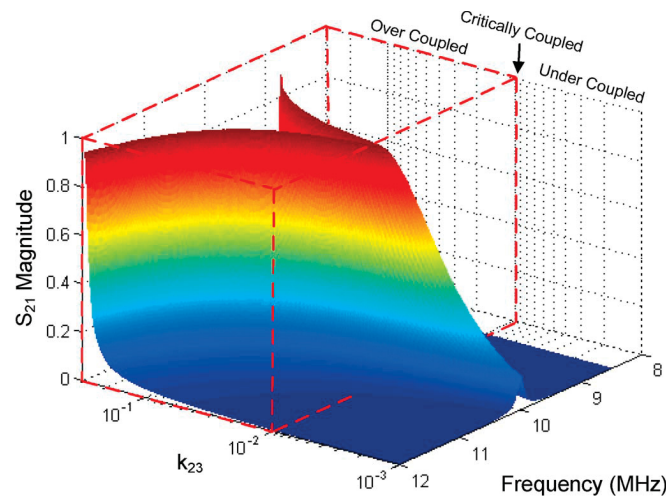

Fig. 3. S_{21} magnitude as a function of frequency and transmitter-to-receiver coupling k_{23} for the simplified circuit model given the values in Table I. The highlighted red volume is the overcoupled regime, where frequency splitting occurs and transfer efficiency can be maintained independent of distance if the correct frequency is chosen.

$$I_4\left(R_{\text{Load}} + R_{P4} + j\omega L_4 + \frac{1}{j\omega C_4}\right) + j\omega I_3 M_{34} = 0 \quad (1)$$

$$k_{xy} = \frac{M_{xy}}{\sqrt{L_x L_y}}, \qquad 0 \leqslant k_{xy} \leqslant 1. \quad (2)$$

These four KVL equations are simultaneously solved for the voltage across the load resistor and yield (3), with the substitution in (4), shown at the bottom of the page.

The system transfer function (3) is plotted in Fig. 3 for the circuit values shown in Table I. This plot shows S_{21} magnitude as a function of frequency and coupling coefficient k_{23}. For consistency, power transfer will be represented in terms of linear magnitude scattering parameters ($|S_{21}|$), which is important experimentally since it can be measured with a vector network analyzer (VNA) for later comparison. The entire wireless power-transfer apparatus can be viewed as a two-port network (one port being the input, fed by the source, and the other being the output, feeding the load). Using (3), one can calculate the equivalent S_{21} scattering parameter using [16], [17], which results in

$$S_{21} = 2\frac{V_{\text{Load}}}{V_{\text{Source}}}\left(\frac{R_{\text{Source}}}{R_{\text{Load}}}\right)^{1/2}. \quad (5)$$

$$\frac{V_L}{V_S} = \frac{i\omega^3 k_{12}k_{23}k_{34}L_2L_3\sqrt{L_1L_4}R_{\text{load}}}{\left(k_{12}^2k_{34}^2L_1L_2L_3L_4\omega^4 + Z_1Z_2Z_3Z_4 + \omega^2\left(k_{12}^2L_1L_2Z_3Z_4 + k_{23}^2L_2L_3Z_1Z_4 + k_{34}^2L_3L_4Z_1Z_2\right)\right)} \quad (3)$$

$$Z_1 = R_{p1} + R_{\text{Source}} + j\omega L_1 - j/(\omega C_1)$$
$$Z_2 = R_{p2} + j\omega L_2 - j/(\omega C_2)$$
$$Z_3 = R_{p3} + j\omega L_3 - j/(\omega C_3)$$
$$Z_4 = R_{p4} + R_{\text{Load}} + j\omega L_4 - j/(\omega C_4) \quad (4)$$

Authorized licensed use limited to: MIT Libraries. Downloaded on November 26,2023 at 23:43:08 UTC from IEEE Xplore. Restrictions apply.

TABLE I
CIRCUIT VALUES USED TO EVALUATE SIMPLIFIED MODEL

PARAMETER	VALUE
R_{source}, R_{Load}	50 Ω
L_1, L_4	1.0 uH
C_1, C_4	235 pF
R_{p1}, R_{p4}	0.25 Ω
K_{12}, K_{34}	0.10
L_2, L_3	20.0 uH
C_2, C_3	12.6 pF
R_{p2}, R_{p3}	1.0 Ω
k_{23}	0.0001 to 0.30
f_0	10 MHz
Frequency	8 MHz to 12 MHz

In Fig. 3, frequency splitting is clearly visible as the value of k_{23} is increased. A SPICE simulation reveals that, indeed, the lower frequency mode of the two coils is in phase, while the higher frequency mode is 180° out of phase. As the coupling between the coils decreases, the frequency separation also decreases until the two modes converge at f_o. This point is called the critical coupling point and represents the farthest distance at which maximum power efficiency is still achievable (since k_{23} is proportional to $1/distance^3$). When k_{23} is greater than k_{critical}, the system is said to be overcoupled, and operating at either resonance will result in maximum power-transfer efficiency. Conversely, when k_{23} is less than k_{critical}, the system is undercoupled, and the amount of power delivered to the load begins to fall off precipitously with distance. The red dashed box outlined in Fig. 3 encloses the "magic regime" where near-constant efficiency versus distance can be achieved if the correct frequency is selected. This is dramatically different from typical far- or near-field systems where efficiency drops off rapidly with distance. An adaptive frequency tuning method, used to ensure that the maximum possible transfer efficiency is achieved at any distance within the "magic regime," is described in Section VI-A.

IV. DERIVATIONS OF CRITICAL COUPLING AND SYSTEM PARAMETERS

Further analysis of the transfer function (3) allows insight into which circuit parameters can be used to optimize the performance of the wireless power system. First, the equation of critical coupling will be derived by substituting the term for series quality factor and resonant frequency, shown in (6), into the transfer function

$$Q_i = \frac{1}{R_i}\sqrt{\frac{L_i}{C_i}} = \frac{\omega_i L_i}{R_i} = \frac{1}{\omega_i R_i C_i} \qquad \omega_i = \frac{1}{\sqrt{L_i C_i}}. \tag{6}$$

Here, the "i_{th}" subscript denotes the circuit elements in Fig. 2, for example, $i = 1$ denotes the elements in the the drive loop (L_1,C_1, and R_{p1}). It should be noted that the expression for ω_i represents the free resonant frequency of each loop and coil, which does not include the damping factor attributed to the resistance in the LCR tank. This approximation has a negligible effect on ω_i and only accounts for a deviation of $\pm 0.25\%$ in the final transfer function. For simplicity, the system is defined to be symmetrical, with the quality factors of the Tx and Rx coils equal $Q_{\text{coil}} = Q_2 = Q_3$ and the quality factors of the Tx and Rx loops equal $Q_{\text{loop}} = Q_1 = Q_4$. The symmetric loop-to-coil coupling $k_{12} = k_{34}$ will be denoted k_{lc}. We will also assume that $R_{\text{source}} = R_{\text{load}}$, $R_{p1} \ll R_{\text{source}}$, $R_{p4} \ll R_{\text{load}}$, and that the uncoupled resonant frequency of each element is defined to be ω_0. To maintain consistency, the notation for the symmetric case, coil-to-coil coupling (k_{23}) will be renamed k_{cc}. Finally, for the sake of brevity, only the derivation for the voltage gain at the center frequency ω_0 is presented in (7). This function represents a 2-D slice of Fig. 3 along the center frequency of 10 MHz, whose apex is the critical coupling point of the system. Furthermore, (7) is equivalent to voltage gain in (3) for $\omega = \omega_0$

$$\left(\frac{V_{\text{Load}}}{V_{\text{Source}}}\right)\bigg|_{\omega=\omega_0} = \frac{i k_{cc} k_{lc}^2 Q_{\text{coil}}^2 Q_{\text{loop}}^2}{k_{cc}^2 Q_{\text{coil}}^2 + (1 + k_{lc}^2 Q_{\text{coil}} Q_{\text{loop}})^2}. \tag{7}$$

In order to find the function that predicts the critical coupling point k_{critical}, the derivative of (7) is taken with respect to k_{cc}. Setting the result to zero and solving for k_{cc} yield (8), where all variables are defined to be positive

$$k_{\text{critical}} = \frac{1}{Q_{\text{coil}}} + k_{lc}^2\, Q_{\text{loop}}. \tag{8}$$

Here, k_{critical} defines the extent of the "magic regime," as shown in Fig. 3. In order to find magnitude at the critical coupling point, k_{critical} is substituted back into k_{cc} in (7). The resulting equation represents the maximum efficiency that is achievable at the furthest possible operation point before the system becomes undercoupled. Using (5) and recalling that $R_{\text{load}} = R_{\text{source}}$, this voltage gain $(V_{\text{Load}}/V_{\text{Source}})$ at the critical coupling point can be converted into the scattering parameters, which will be denoted $|S_{21}|_{\text{critical}}$ in

$$|S_{21}|_{\text{critical}} = \frac{k_{lc}^2 Q_{\text{coil}} Q_{\text{loop}}}{1 + k_{lc}^2 Q_{\text{coil}} Q_{\text{loop}}} = \frac{k_{lc}^2 Q_{\text{loop}}}{k_{\text{critical}}}. \tag{9}$$

Recall that, in order to maximize range, we must minimize k_{critical} because this increases the extent of the "magic regime," which spans from k_{critical} to 1.0. Examining (8) shows that reducing k_{lc} lowers k_{critical} and therefore increases range. However, according to (9), reducing k_{lc} also reduces efficiency. Indeed, the choice of k_{lc} trades off the efficiency level in the "magic regime" (height of the V-shaped ridge) versus the extent of the "magic regime" (spatial length of V-shaped ridge). Fig. 4 shows a plot of this tradeoff curve $|S_{21}|_{\text{critical}}$ versus k_{critical}, as a function of the common parameter k_{lc}.

The area under this tradeoff curve serves as a useful figure of merit (FOM) for system performance. An optimal wireless power system, which could losslessly deliver power at an infinite range $(coupling \to 0)$ would have a FOM of unity. For the symmetrical case, the FOM integral can be evaluated

Authorized licensed use limited to: MIT Libraries. Downloaded on November 26,2023 at 23:43:08 UTC from IEEE Xplore. Restrictions apply.

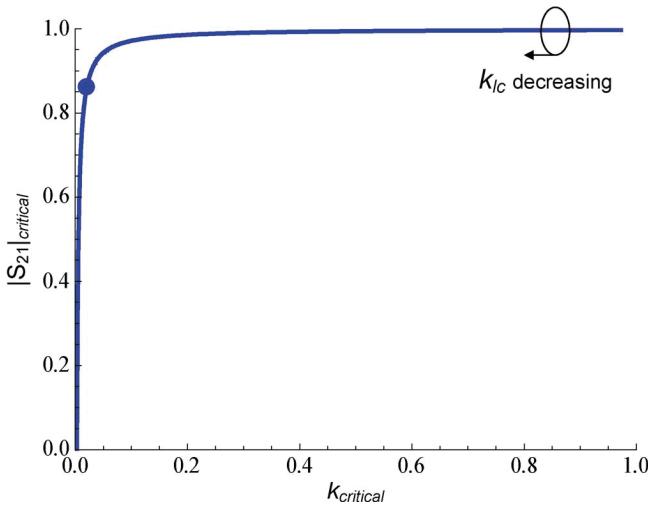

Fig. 4. Efficiency versus critical coupling range: $|S_{21}|_{\text{critical}}$ versus k_{critical} tradeoff curve as a function of the tuning parameter k_{lc}, with our system's operating point indicated (large dot at $k_{lc} = 0.135$).

analytically. Assuming that $Q_{\text{coil}} > 1$, the area under the tradeoff curve is

$$FOM = \int_0^1 |S_{21}|_{\text{critical}} dk_{\text{critical}} = 1 - \frac{1}{Q_{\text{coil}}} - \frac{\ln Q_{\text{coil}}}{Q_{\text{coil}}}. \tag{10}$$

The FOM is only dependent on Q_{coil} and is independent of Q_{loop}. The quality factor of the resonators (coils) entirely determines this measure of system performance, which approaches unity in the limit of infinite Q_{coil}. The measured Q_{coil} values for our system are around 300 and 400, corresponding to $FOM =$ .978 and $FOM =$ .982. Choosing a feasible value of Q_{loop} is the next important design question. To derive a guideline, we will find an expression for the "knee" of the range–efficiency tradeoff curve, which is defined as the point at which the slope equals unity in Fig. 4. Solving $d|S_{21}|_{\text{critical}}/dk_{\text{critical}} = 1$ for k_{critical}, we find

$$k_{\text{criticalknee}} = Q_{\text{coil}}^{-1/2}. \tag{11}$$

If Q_{loop} is too small, then even when setting k_{lc} to its maximum value of 1.0, k_{critical} will not be able to reach $k_{\text{criticalknee}}$. To find the minimum necessary Q_{loop} value, we can solve (8) for Q_{loop} with $k_{\text{critical}} = k_{\text{criticalknee}}$ and $k_{lc} = 1$, which yields $Q_{\text{loop}} = (Q_{\text{coil}}^{1/2} - 1)Q_{\text{coil}}^{-1} \approx Q_{\text{coil}}^{-1/2}$ for large Q_{coil}. Specifically, a good operating point on the tradeoff curve should be achievable as long as $Q_{\text{Loop}} > Q_{\text{coil}}^{-1/2}$. For $Q_{\text{coil}} = 300$, this condition becomes $Q_{\text{loop}} > 0.06$. In our working system, the loaded Q_{loop} values are around 0.9, about one order of magnitude larger than this limit.

The key conclusion is that Q_{Coil} determines system performance (as measured by our FOM), as long as a minimum threshold value of Q_{loop} is exceeded. The actual value of Q_{loop} (less than one for our system) is dominated by the source and load impedances. The larger the Q_{Coil} is, the smaller is the required minimum Q_{loop}. Conversely, moving to a more demanding load (with Q_{loop} below the current threshold value) could be accomplished by sufficiently increasing Q_{Coil}.

Fig. 5. Photograph of the transmitter and receiver used in wireless power system. Outside diameter of the large coils is 59 cm.

V. Model Validation and Experimental Results

Fig. 5 shows the experimental setup used to validate the theoretical model. The transmitter on the left consists of a small drive loop centered within a flat spiral transmit resonator. The drive loop is 28 cm in diameter, with a series-connected variable capacitor used to tune the system to 7.65 MHz. A SubMiniature type-A (SMA) connector is also placed in series so that an RF amplifier can drive the system, as depicted in the circuit diagram in Fig. 2. The large transmit coil starts with an outer diameter of 59 cm and spirals inward with a pitch of 1 cm for approximately six turns. The resonant frequency of 7.65 MHz was determined experimentally and is not intended to correlate with the resonant frequency of the mathematical example in Section III. Since it is difficult to accurately predict the self-capacitance of the coils, the resonant frequency is tuned by manually trimming the end of the spiral until each coil individually resonates at 7.65 MHz. The receiver is constructed similarly. All elements are made of 2.54-mm-diameter copper wire, supported by Plexiglas armatures.

One of the significant challenges when comparing the theoretical model to the measured data is the accurate estimation of the lumped circuit parameters (L, C, and R) of the physical system. To accomplish this task, we used standard RF and microwave measurement techniques developed to extract parameters such as resonant frequency, coupling coefficient, and unloaded Q factor from resonant structures [18].

A VNA is used to measure the scattering parameters of a device under test (DUT) as a function of frequency. Next, an impedance model of the DUT is fitted to the complex S_{11} data using an unconstrained nonlinear optimization routine to solve for the free variables. Since a VNA can sample a large number of data points, the problem is overdetermined, allowing for a reliable fit with error estimation.

In the case of the drive and receive loops, the values for L, C, and R_p can be determined directly. However, when evaluating the coils, it is not possible to disambiguate inductance and resistance, and as a result, parameter extraction of the coils is in terms of resonant frequency, coupling coefficient, and unloaded Q factor. For the sake of completeness, Neumann's formula [19], [20] is used to calculate the coils' inductance, and the equation for quality factor (6) is used to determine

Authorized licensed use limited to: MIT Libraries. Downloaded on November 26,2023 at 23:43:08 UTC from IEEE Xplore. Restrictions apply.

TABLE II
MEASURED LUMPED ELEMENT VALUES FOR EACH INDIVIDUAL CIRCUIT ELEMENTS OF EXPERIMENTAL TRANSMITTER AND RECEIVER

TRANSMITTER		RECEIVER	
COMPONENT	VALUE	COMPONENT	VALUE
L_1	0.965 uH	L_4	0.967 uH
C_1	449.8 pF	C_4	448.9 pF
R_{p1}	0.622 Ω	R_{p4}	0.163 Ω
R_{source}	50 Ω	R_{load}	50 Ω
Q_1	0.91	Q_4	0.93
F_1	7.64 MHz	F_4	7.64 MHz
K_{12}	0.1376	K_{34}	0.1343
Q_2	304.3	Q_3	404.4
F_{o2}	7.66 MHz	F_{o3}	7.62 MHz
L_2	39.1 uH	L_3	36.1 uH
C_2	11.04 pF	C_3	12.10 pF
R_{p2}	6.19 Ω	R_{p3}	4.27 Ω

the resistance. However, the model validation could equally be done using the Q form of the transfer function. The coefficient of determination (R^2) is used to quantify the quality of the fit, where $0 < R^2 < 1$ with a value 1 indicating a perfect match between the fitted model and measurements. A summary of the extracted parameters for each of the individual elements from the experimental setup depicted in Fig. 5 is shown in Table II. All of the parameters extracted had an R^2 value of over 0.9999, which indicates, with high confidence, that the values model the system accurately.

The process of comparing the theoretical model of the wireless power system to measured results will be presented in two steps. First, Section V-A and B use extracted values for coupling coefficient k_{23} from the complex S_{21} data to validate the circuit model that is independent of coupling (i.e., k_{23} is the only unknown variable from Table II and is extracted from the overdetermined S_{21} measurements). Second, Section V-C uses Neumann's formula to predict all of the coupling coefficients in the system, thus enabling a full prediction of system performance using only the lumped circuit values from Table II.

In the experiment, the transmitter and receiver (shown in Fig. 5) are placed facing each other along their common axis. This is shown in Fig. 8, which represents the top view of the experimental setup. Ports one and two of a VNA are connected to the drive and load loops, respectively. Thus, the source and load resistance of the system is 50 Ω. The drive loop and Tx coil are set a fixed distance apart (13.5 cm), thus keeping k_{12} constant. The Rx coil and load loop are similarly fixed at 13.5 cm. Finally, the receiver (as a single unit) is moved away from the transmitter along the common axis. The S_{21} scattering parameters are recorded every 5 cm, from 10 to 130 cm.

A. Effects of Parasitic Cross-Coupling

Fig. 6 shows experimentally the measured $|S_{21}|$ data to the ideal model in (3) and to a more complete asymmetric model that includes parasitic cross-coupling terms (k_{13}, k_{24}, and k_{14}). The agreement between the complete model and the experimental data is excellent. The difference in the magnitude of the

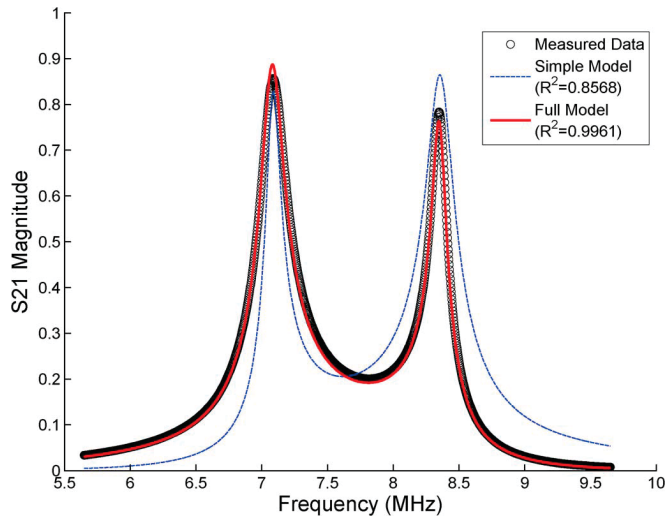

Fig. 6. Diagram depicting the top view of the experimental setup, where the receiver, as a single unit, is moved away from the transmitter. In this experiment, the free variable is the coil-to-coil coupling (k_{23}), which varies as a function of the distance between the coils.

$|S_{21}|$ peaks for the upper and lower modes can be explained by considering the phase of the two modes.

Based on the dynamics of coupled resonators [15], one expects that, in the lower frequency mode, the current in the transmit coil should be in phase with the current in the receive coil; in the higher frequency mode, the coil currents should be antiphase (180° out of phase). In the lower mode, in which the Tx and Rx coils are in phase, the parasitic feed-through from the drive loop to the Rx coil (associated with coupling constant k_{13}) contributes constructively to the magnitude of the current in the receive coil. In the upper mode, the Rx coil phase is inverted, but the parasitic feed-through is not; thus, the feed-through interferes destructively with the Rx coil current. Similar arguments apply to the other parasitic couplings. The fact that the magnitudes of the mode differences are modeled well only when parasitic couplings are included (as shown in Fig. 6) supports this conclusion.

A discrete matching network or shielded transformer could be used to directly connect the source/load to the coils. This would eliminate the cross-coupling term, simplify the model, and, possibly, also simplify system construction. On the other hand, the parasitic feed-through benefits system performance in the lower mode, and this benefit would be lost by eliminating the drive and load loops.

B. Model With Extracted Coupling Coefficient Versus Measured Data

Fig. 7 shows a 3-D plot of measured S_{21} data in linear magnitude form, depicted by black dots. These dots form striped rows, each of which corresponds to a frequency sweep of data points taken with a VNA. Each row of dots (or frequency sweep) represents a VNA measurement taken every 5 cm as the receiver is moved away from the transmitter. The mesh underneath the measured data represents the transfer function of the circuit model using extracted and interpolated values for

Authorized licensed use limited to: MIT Libraries. Downloaded on November 26,2023 at 23:43:08 UTC from IEEE Xplore. Restrictions apply.

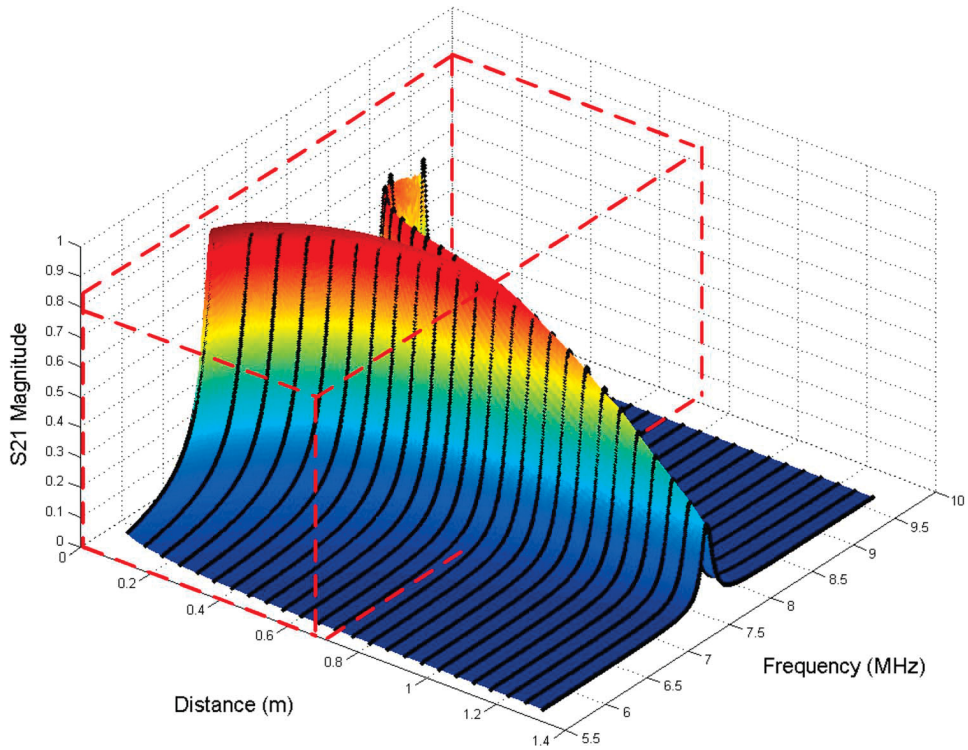

Fig. 7. Comparison of (black dots) experimental data to the (dotted blue line) simplified transfer function and to the (red line) complete transfer function. The simple model neglects parasitic cross-coupling (e.g., k_{13}, k_{24}, and k_{14}) and does not reproduce the amplitude difference between the upper and lower modes. The complete model reproduces this amplitude difference, which is explained by the phase of the parasitic coupling terms (k_{13} and k_{24}) relative to the nonparasitic terms (e.g., k_{23}) for the two resonant modes.

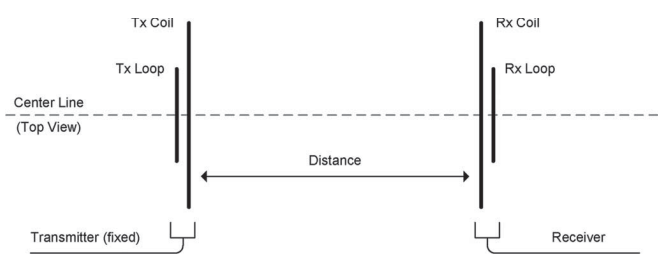

Fig. 8. (Black dots) Measured $|S_{21}|$ data plotted in magnitude form. Each row of black dots represents a frequency sweep taken by the VNA every 5 cm as the receiver was moved away from the transmitter. The mesh underneath the data is the theoretical model.

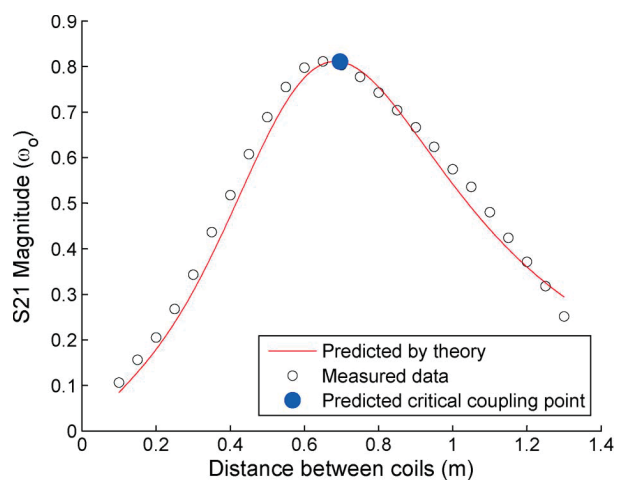

Fig. 9. Predicted behavior of the wireless power system at the resonant frequency f_o using Neumann's formula, along with the (blue dot) predicted critical coupling point and S_{21} measured data.

coupling coefficients. Frequency splitting, the point of critical coupling, and damping are clearly visible. For each of the frequency sweeps, R^2 was calculated to quantify the correspondence between theory and measurements. The average R^2 value for the 25 measurements is 0.9875. It is important to note that both Figs. 6 and 7 show a slight underprediction for the high-frequency mode and a slight overprediction for the low-frequency mode. This is believed to be due to capacitive detuning and/or capacitive coupling (which is not modeled) and becomes more significant at close range.

C. Model With Calculated Coupling Coefficients Versus Measured Data

In the preceding section, the model was compared to measured data for discrete values of coupling coefficient. Since the circuit model itself does not explicitly model distance, it is necessary to calculate the coupling between each inductive element as a function of distance. In the following analysis, these calculated values of coupling coefficients, along with the L, C, and R values listed in Table II, are inserted into the transfer function of the full system and compared to measured results. In order to present a clean comparison of theory and measured results, Fig. 9 shows the magnitude of the measured scattering parameter ($|S_{21}|$), as a function of system distance, at the center frequency ($f_o = 7.65$ MHz). When the distance

Authorized licensed use limited to: MIT Libraries. Downloaded on November 26,2023 at 23:43:08 UTC from IEEE Xplore. Restrictions apply.

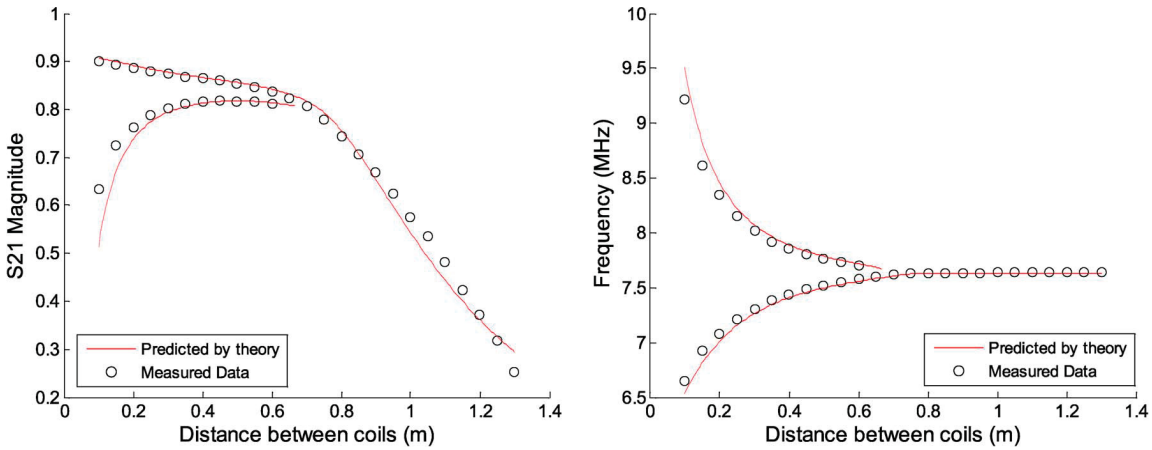

Fig. 10. Calculated and measured frequency splitting values plotted as a function of distance. The S_{21} magnitude of the two modes is shown on the left, and the frequency of the two modes is shown on the right.

between the transmitter and receiver is small, the system is overcoupled, and the magnitude of the power transferred is small at this operating frequency. This is a result of frequency splitting, which causes resonant modes at frequencies higher and lower than the center frequency of ω_o. As the distance is increased, the system becomes critically coupled, and the magnitude is at its highest. As the distance between the coils is further increased, the system becomes undercoupled, and the magnitude of the transferred power begins to fall. The calculated red line of system performance in Fig. 9 shows a good match with the measured data. The blue marker on the plot shows the predicted value for the critical coupling point, using the asymmetrical form of (8) and (9), along with Neumann's formula to calculate the distance from coupling coefficient k_{23}.

Frequency splitting is further investigated in Fig. 10, which shows the calculated and measured magnitudes for each mode of the system as a function of distance (left) along with the resonant frequency of each mode as a function of distance (right). Here, the derivative of the transfer function is taken with respect to ω and set to zero to calculate the maximum magnitude for a given distance. The discontinuity in the prediction of the high-frequency branch occurs when the two modes begin to merge near the critical coupling point. This results in a nonzero slope for the peaks of the smaller high-frequency mode, and thus, the derivative does not reach zero. Here, the circuit model plus Neumann's formula shows a good prediction of the performance of the wireless power system. The magnitude versus frequency plot in Fig. 10 shows a noticeable underprediction for the high-frequency mode at small distances. The authors believe this is caused by capacitive detuning having a more pronounced effect as the transmitter and receiver are moved very close to each other.

VI. Adaptive Tuning for Range-Independent Maximum Power Transfer

A necessary component for a compelling wireless power system is the ability to operate at a multitude of distances and orientations without the need for precision manual tuning.

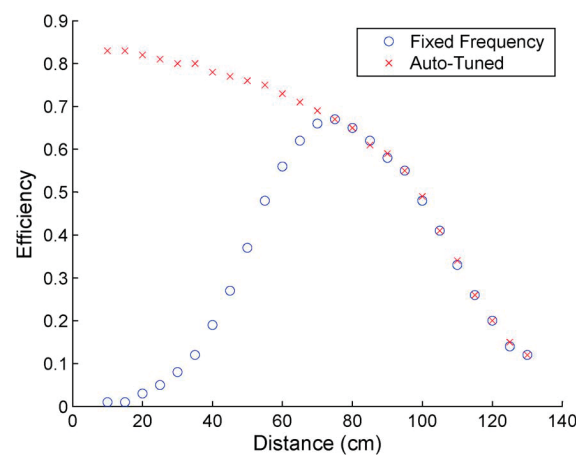

Fig. 11. Automatic frequency tuning compared to a fixed drive frequency as a function of distance between the transmitter and receiver.

A. Automatic Frequency Tuning

Using the frequency splitting presented here, it is possible to design a system that automatically adjusts to provide maximum possible efficiency as a user moves the receiver to locations within the system's working range (i.e., $k_{23} > k_{\text{critical}}$). Introducing a directional coupler between the amplifier and drive loop, as shown in Fig. 1, allows the transmit system to continuously measure the incident and reflected powers as a function of frequency. Since this system forms a transmission line, the power not consumed by the load or lost to parasitic resistance is reflected back to the source.

Fig. 11 shows a graph of transfer efficiency versus distance for the fixed-frequency case of $f_o = 7.65$ MHz, and the automatic-frequency-tuning case. The experiment is done in the same manner as the VNA measurements in the previous section. The receiver was incrementally moved away from the transmitter along the system's common axis; the source resistance was the 50-Ω amplifier/decoupler, and the load resistance was a 50-Ω RF power meter. In this case, the transmitted power was 30 W, as opposed to the signal level measurements done with the VNA. In Fig. 11, the fixed-frequency data points show the same trends with the measurements made with the VNA in

Authorized licensed use limited to: MIT Libraries. Downloaded on November 26,2023 at 23:43:08 UTC from IEEE Xplore. Restrictions apply.

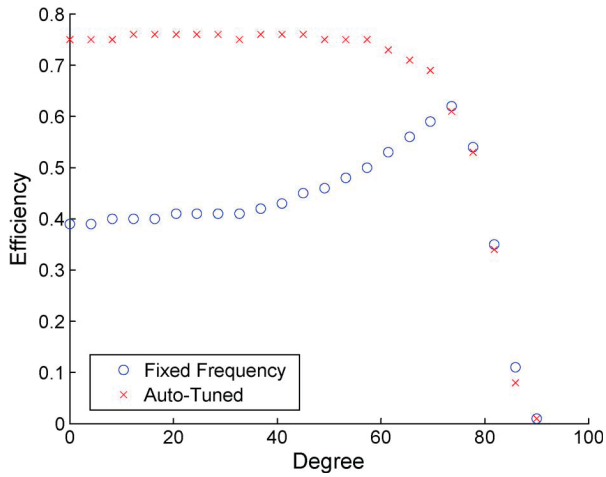

Fig. 12. Automatic frequency tuning compared to a fixed drive frequency as a function of the angle between the transmitter and receiver. An angle of 0° corresponds to the coils facing each other, while 90° corresponds to the receiver perpendicular to the transmitter. The transmitter-to-receiver spacing is 0.5 m.

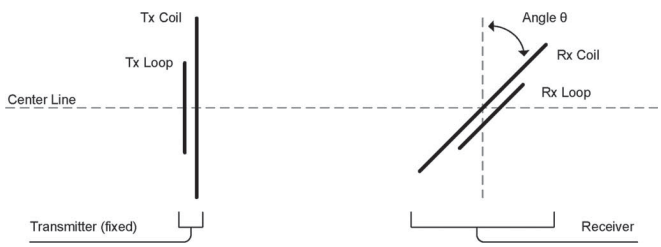

Fig. 13. Diagram depicting the top view of the experimental setup, where the orientation of the receiver is varied by angle θ at a fixed distance from the transmitter.

Fig. 9. When the frequency tuning is enabled, the controller picks the maximum resonant peak and tracks it as the receiver is moved away from the transmitter. The plot shows that at short ranges the system is very efficient compared to the fixed-frequency case. As distance is increased, the efficiency decreases slowly until the critical coupling point, where the two modes merge and the system returns to the undercoupled regime.

One of the key principles of this system is that frequency splitting is a function of the coil-to-coil coupling coefficient. In the aforementioned analysis, we show how the coupling, and therefore the power transfer, varies as a function of distance along the transmission axis. The coupling will also vary with orientation. As long as the receiver is sufficiently close to the transmitter, almost any orientation and/or position will cause some amount of mutual inductance between the two coils. If this mutual inductance results in sufficient coupling (i.e., $k_{23} > k_{\text{critical}}$), automatic frequency tuning can be used to find the frequency that will result in the highest possible transfer efficiency. To demonstrate orientation independence, Fig. 12 shows a plot of power-transfer efficiency versus orientation as the receiver is rotated from 0° to 90°, for both fixed-frequency and auto-tuned operation. Here, the receiver unit is placed on axis at a fixed distance of 50 cm, as shown in Fig. 13. As the receive coil is rotated, the amount of magnetic flux that passes through the opening of the coil decreases. Thus, the fixed-frequency case experiences the same trend of transitioning from

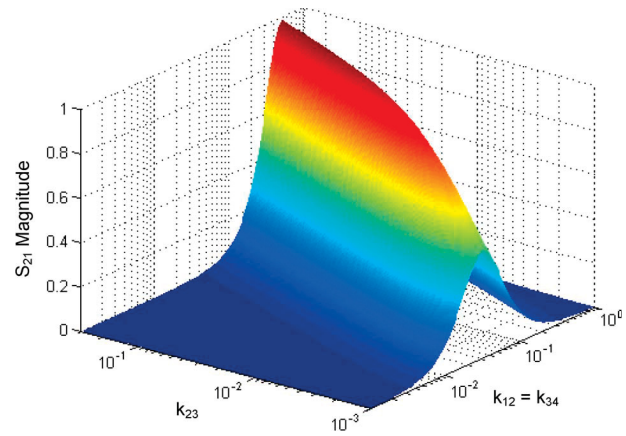

Fig. 14. $|S_{21}|$ as a function of k_{23} and k_{12}.

the overcoupled to critically coupled to undercoupled regimes as in the previous examples. When frequency tuning is applied, a nearly constant efficiency can be obtained until the receiver is rotated past 65°.

B. Impedance Adaptation Techniques for Narrow-Band Operation

For regulatory reasons, it may be desirable for the wireless power system to be able to function in a narrower band than the frequency tuning systems described so far. For example, one might want the wireless power system to stay inside an industrial, scientific, and medical band. This section describes narrow-band wireless power-transfer schemes that can support range and orientation adaptation by tuning system parameters other than frequency.

Rather than considering k_{lc} to be a static design parameter to be optimized (as previously mentioned), one can consider it as a dynamically variable impedance matching parameter that can enable range adaptation without frequency tuning. Fig. 14 shows a plot of S_{21} magnitude as a function of k_{23} and k_{lc} (for symmetric loop-to-coil coupling). This figure shows that adapting the loop-to-coil coupling to compensate for a nonoptimal k_{23} is another method for adapting to varying range and orientation.

If the system is driven at ω_0 and the wireless power system is operating in the overcoupled regime ($k_{23} > k_{\text{critical}}$), frequency splitting will result in the system being off resonance, and little to no power will be transferred. To bring the efficiency of the system back to a maximum, k_{lc} can be decreased, causing k_{critical} in (8) to decrease, until $k_{23} = k_{\text{critical}}$, at which point maximum power transfer can resume. In a laboratory demonstration, we have successfully implemented a form of this tuning method that allows tuning for a variety of Tx–Rx distances (k_{23} values) with a hand adjustment of a loop that can be rotated about its coil, thereby changing k_{lc}. The k_{lc} adaptation method has the advantage of allowing operation at a single frequency ω_0, which would be advantageous for band-limited operation. Thus, it is of practical interest to develop electronically controllable techniques for k_{lc} tuning. As noted earlier, the system's loops could be replaced by discrete matching networks; making these matching networks electronically variable could allow for automatic k_{lc} tuning.

Authorized licensed use limited to: MIT Libraries. Downloaded on November 26,2023 at 23:43:08 UTC from IEEE Xplore. Restrictions apply.

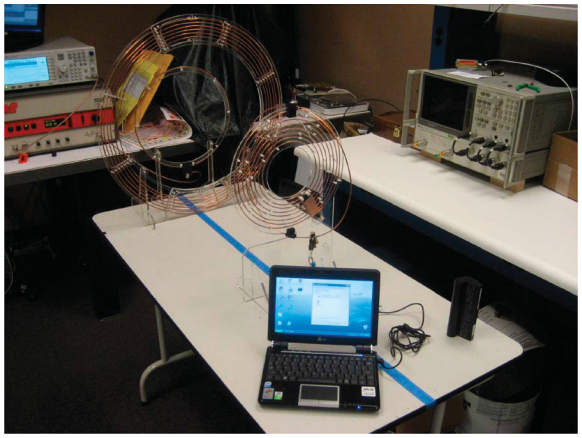

Fig. 15. Wirelessly powered laptop computer. The battery has been removed and is visible in the lower right of the table. The wireless power system is able to provide all of the laptop's peak power consumption of 12 W at a range of 0.7 m. Including the rectifier (which has not yet been optimized), the system efficiency (measured from amplifier output through the laptop) is 50%.

VII. Conclusion

Magnetically coupled resonant structures offer a unique set of benefits, as well as design challenges, when used for wireless power transfer. One of the remarkable results is the existence of the "magic regime," where efficiency remains nearly constant over distance, as long as the receiver is within the operating range of the transmitter. This is not the case for conventional far- and near-field wireless power systems, whose efficiencies decline sharply with range.

The work in this paper has provided a deeper understanding of the underlying principles of coupled magnetic resonance, as well as a simple circuit model of the system. A derivation of the transfer function of this model reveals which concepts play a critical role in system performance: frequency splitting, operating range, and impedance matching. In order to accurately characterize the wireless power system, measurement techniques that use a network analyzer for circuit parameter extraction have been implemented. Excellent agreement between the circuit model and measurements has been demonstrated, with a coefficient of determination of 0.9875. Lastly, the issue of receiver alignment sensitivity is addressed with an adaptive tuning algorithm. We demonstrate that, for any receiver position and/or orientation, a frequency can be identified, which maximizes power-transfer efficiency. In addition, a tracking algorithm allows for the peak efficiency to be maintained as the receiver is moved in space.

One compelling usage scenario is a workspace where devices, such as laptops, cell phones, and Universal Serial Bus peripherals, are seamlessly powered and recharged as easily as data are transmitted through the air. As a final demonstration of the potential of this type of wireless power system, Fig. 15 shows a laptop being continuously powered via the magnetically coupled resonators. Here, the laptop battery has been removed, and the wireless power system is providing all the power needed for operation. The signal generator, amplifier, and directional coupler can be seen in the background (top left corner) and are controlled by a computer. The amplifier drives the same 28-cm transmit loop and 59-cm transmit coil from the early experiments. The receiver is placed 0.7 m for the transmitters and consists of a smaller 28-cm coil and a 30-cm loop, seen in the foreground. A simple bridge rectifier is used to provide dc power to the modified laptop power brick. In this demonstration, the removed battery is visible, placed next to the laptop (lower right). The RF-amplifier-output-to-dc-laptop-input efficiency is 50% (which includes the efficiency of the nonoptimized rectifier and power brick).

VIII. Future Work

From the circuit model and derivation of critical coupling, it is clear that maximizing the coil's quality factor, as well as proper loading of the drive and load loops, can result in improved range and efficiency. Furthermore, the impedance matching between the loop and coil embodied by the coupling constant k_{lc} suggests that a discrete matching network can be used to directly connect the source/load to the coils, thereby simplifying the system.

Clearly, the advantages of high and near-constant transfer efficiency at mid-range distance compared to near- and far-field techniques make this technology exciting for many applications. There are any number of low-power wireless recharging scenarios that would benefit from increased range versus efficiency at power levels typically used in RFID. Finally, this paper has focused on the delivery aspect of RF power while consumer electronics require dc power for operation and recharging. Adaptive rectifier designs will need to be developed that do not interfere with the operation of the magnetically coupled resonators.

References

[1] S. Ahson and M. Ilyas, *RFID Handbook: Applications, Technology, Security, and Privacy*. Boca Raton, FL: CRC Press, 2008.

[2] A. Sample, D. Yeager, P. Powledge, A. Mamishev, and J. Smith, "Design of an RFID-based battery-free programmable sensing platform," *IEEE Trans. Instrum. Meas.*, vol. 57, no. 11, pp. 2608–2615, Nov. 2008.

[3] W. Brown, "The history of power transmission by radio waves," *IEEE Trans. Microw. Theory Tech.*, vol. MTT-32, no. 9, pp. 1230–1242, Sep. 1984.

[4] J. McSpadden and J. Mankins, "Space solar power programs and microwave wireless power transmission technology," *IEEE Microw. Mag.*, vol. 3, no. 4, pp. 46–57, Dec. 2002.

[5] A. Sample and J. Smith, "Experimental results with two wireless power transfer systems," in *Proc. IEEE RWS*, Jan. 2009, pp. 16–18.

[6] PowerMat Inc., Nov. 2009. [Online]. Available: http://www.powermat.com

[7] A. Karalis, J. Joannopoulos, and M. Soljacic, "Efficient wireless non-radiative mid-range energy transfer," *Ann. Phys.*, vol. 323, no. 1, pp. 34–48, 2008, January Special Issue 2008.

[8] A. Kurs, A. Karalis, R. Moffatt, J. D. Joannopoulos, P. Fisher, and M. Soljacic, "Wireless power transfer via strongly coupled magnetic resonances," *Science*, vol. 317, no. 5834, pp. 83–86, Jul. 2007.

[9] B. Cannon, J. Hoburg, D. Stancil, and S. Goldstein, "Magnetic resonant coupling as a potential means for wireless power transfer to multiple small receivers," *IEEE Trans. Power Electron.*, vol. 24, no. 7, pp. 1819–1825, Jul. 2009.

[10] C. Zhu, K. Liu, C. Yu, R. Ma, and H. Cheng, "Simulation and experimental analysis on wireless energy transfer based on magnetic resonances," in *Proc. IEEE VPPC*, Sep. 2008, pp. 1–4.

[11] Z. N. Low, R. Chinga, R. Tseng, and J. Lin, "Design and test of a high-power high-efficiency loosely coupled planar wireless power transfer system," *IEEE Trans. Ind. Electron.*, vol. 56, no. 5, pp. 1801–1812, May 2009.

[12] J. Casanova, Z. N. Low, and J. Lin, "A loosely coupled planar wireless power system for multiple receivers," *IEEE Trans. Ind. Electron.*, vol. 56, no. 8, pp. 3060–3068, Aug. 2009.

Authorized licensed use limited to: MIT Libraries. Downloaded on November 26,2023 at 23:43:08 UTC from IEEE Xplore. Restrictions apply.

[13] Y.-H. Kim, S.-Y. Kang, M.-L. Lee, B.-G. Yu, and T. Zyung, "Optimization of wireless power transmission through resonant coupling," in *Proc. CPE*, May 2009, pp. 426–431.
[14] A. Woodruff, K. Anderson, S. Mainwaring, and R. Aipperspach, "Portable, but not mobile: A study of wireless laptops in the home," *Proc. Pervasive*, pp. 216–233, May 2007.
[15] N. Fletcher and T. Rossing, *The Physics of Musical Instruments*. Berlin, Germany: Springer-Verlag, 1998.
[16] R. Mongia, *RF and Microwave Coupled-Line Circuits*. Norwood, MA: Artech House, 2007.
[17] J. Chen, *Feedback Networks: Theory and Circuit Application*. Singapore: World Scientific, 2007.
[18] D. Kajfez and E. Hwan, "*Q*-factor measurement with network analyzer," *IEEE Trans. Microw. Theory Tech.*, vol. MTT-32, no. 7, pp. 666–670, Jul. 1984.
[19] J. O'Loughlin, "Circuit and electromagnetic system design notes, note 42," Univ. New Mexico, Albuquerque, NM, 1998.
[20] H. Chan, K. Cheng, and D. Sutanto, "A simplified Neumann's formula for calculation of inductance of spiral coil," in *Proc. 8th Int. Conf. Power Electron. Variable Speed Drives (IEE Conf. Publ. No. 475)*, 2000, pp. 69–73.

Alanson P. Sample (S'03) received the B.S. and M.S. degrees in electrical engineering from the University of Washington (UW), Seattle, in 2005 and 2008, respectively, where he is currently working toward the Ph.D. degree in electrical engineering.

As an undergraduate, he worked in the Sensors Energy and Automation Laboratory, UW, where he coauthored several papers on autonomous robotic power cable inspection. Throughout his graduate studies, he has worked closely with Intel Labs Seattle (formerly Intel Research Seattle), Seattle, where he has held numerous internships and is currently employed as part of a multiyear contract. He has published several papers on his work related to the Wireless Identification and Sensing Platform. His research interests lie broadly in the area of wireless power, including antenna theory and design, energy harvesting from ambient and deliberate sources, wirelessly powered systems containing sensing and computing elements, and the applications of these systems.

Mr. Sample was a recipient of the Granger Foundation Fellowship in 2006.

David A. Meyer (S'10) was born in Tarzana, CA, on September 10, 1987. He received the B.S. degree in physics and electrical engineering from the University of Washington, Seattle, WA, in 2009. He is currently working toward the Ph.D. degree in electrical engineering at Massachusetts Institute of Technology (MIT), Cambridge.

He completed a research experience for undergraduates at the University of Washington in Summer 2007 and another at the University of Colorado, Boulder, in Summer 2008. During the 2008–2009 school year, he worked with Intel Labs Seattle and stayed on as an Intern during the summer. He is currently an Interdisciplinary Quantum Information Science and Engineering (iQuISE) Fellow at MIT.

Mr. Meyer is a member of Eta Kappa Nu.

Joshua R. Smith (M'99) received the B.A. degrees in computer science and in philosophy from Williams College, Williamstown, MA, the M.A. degree in physics from the University of Cambridge, Cambridge, U.K., and the Ph.D. and S.M. degrees from the MIT Media Laboratory, Cambridge, MA.

He is currently a Principal Engineer with Intel Labs Seattle, Seattle, WA, where he leads research in wireless power and robotics. He holds affiliate faculty appointments in the Departments of Electrical Engineering and Computer Science and Engineering, University of Washington, Seattle. His research interests include all aspects of sensor systems, including the development of novel sensor systems; power, communication, signal processing, and security issues in sensor systems; and algorithms and applications that use data from novel sensor systems. His research has application in the fields of robotics, ubiquitous computing, and human–computer interaction. Previously, he coinvented an electric-field-based passenger-sensing system that is used to suppress unsafe airbag deployment in all Honda cars.

Authorized licensed use limited to: MIT Libraries. Downloaded on November 26,2023 at 23:43:08 UTC from IEEE Xplore. Restrictions apply.